Research on The Bonding Properties of Vitrified Bonds With Porous Diamonds and The Grinding Performance of Porous Diamond Abrasive Tools

Jianwei LI
Hunan University College of Materials Science and Engineering
Wenjun FANG
Hunan University State Key Laboratory of Advanced Design and Manufacturing for Vehicle Body
Long WAN (WanLong1956@163.com)
Hunan University College of Materials Science and Engineering
Xiaopan LIU
Hunan University College of Materials Science and Engineering
Weida HU
Hunan University of Technology Liling ceramic institute
Dan CAO
Hunan University College of Materials Science and Engineering
Kai HAN
Hunan University College of Materials Science and Engineering
Yingying LI
Shangqiu Institute of Technology
Yonggao YAN
state key laboratory of advanced technology for materials synthesis and processing, Wuhan University of Technology

Research Article

Keywords: Vitrified bonds, Porous diamonds, Wettability, Abrasive tools, Grinding

Posted Date: October 26th, 2021

DOI: https://doi.org/10.21203/rs.3.rs-970850/v1

Version of Record: A version of this preprint was published at Diamond and Related Materials on January 1st, 2022. See the published version at https://doi.org/10.1016/j.diamond.2022.108841.

Abstract

Ordinary diamond presents the disadvantages of poor self-sharpening and concentrated grinding stress when it is used as an abrasive. Moreover, this kind of diamond cannot be well wetted by the vitrified bond, resulting in a lower holding force of the binder to the abrasives (i.e., the diamond is easy to detach from the binder matrix during grinding). These comprehensive factors not only reduce the surface quality of the processed workpiece, but also hinder the processing efficiency. In order to solve these problems, a new type of porous diamond with high self-sharpening properties was prepared using a thermochemical corrosion method in this study. Our results showed a great improvement in pore volume and specific surface area of the porous diamond compared with ordinary diamond abrasive particles, and the holding force and wettability of vitrified bond to the porous diamond abrasive particles were also improved. Compared with ordinary diamond abrasive tools, porous diamond abrasive tools showed a 29.6% increase in grinding efficiency, a 15.5% decreased in grinding ratio, a 27.5% reduction in workpiece surface roughness, and the scratches on the silicon wafer surface were reduced and refined.

1. Introduction

The advantages of diamonds include high wear resistance, high thermal conductivity and high hardness. They are often mixed with vitrified bonds to prepare abrasive tools for grinding hard brittle materials such as glass, ceramics, gemstones, stone and hard alloys [1–4]. With the advancement of science, the grinding of silicon wafers and other new materials now demand higher quality, higher precision and higher efficiency [5–7]. Due to the small size of ordinary diamonds, it is usually necessary to use a binder to combine them together to produce grinding tools with a certain size, shape and strength [8]. However, the smooth diamond surface is chemically inert, and the bonding strength between diamonds and vitrified bonds is very low. The diamonds easily detach during grinding and the effective utilization rate of diamonds is very low, which greatly reduces the service life of abrasive tools [9, 10]. Moreover, ordinary diamonds often expose only one large cutting edge after being prepared into abrasive tool, and the self-sharpening property of diamonds is poor. During precision machining, the grinding stress of ordinary diamonds is concentrated, and the surface of the workpiece is severely scratched, which greatly reduces the grinding accuracy of the grinding tool [11–13].

In order to increase holding force of binder on diamonds and improve the self-sharpening property of diamonds, many researchers have carried out in-depth studies. The studies have shown that some coatings (Ti, Cr, TiO_2, V_2O_5 etc.) chemically bonded with diamonds, which increased the wettability of the binder to the diamonds and improved the holding force of the binder on the diamonds [8, 14–16]. Some researchers have carried out metal catalytic hydrogenation corrosion and oxygen plasma corrosion studies on diamond surfaces, resulting in micro patterns (pits and bulges) on the diamond surfaces, which effectively increased the holding force of the binder on the diamonds [17, 18]. The above methods do improve the holding force of the binder on diamonds, but they do not change the self-sharpening property of diamonds and the machining efficiency has not been improved. Impressively, large size single particle porous diamonds were prepared on seed diamonds that were mixed with a micron/submicron-

scale diamond powders and metal catalyst powders when combined using high-pressure and high-temperature techniques [19]. This method produced a new type of diamond with a porous skeleton structure, which improved the self-sharpening property of the diamond. However, the synthesis conditions of this method were relatively high (at 5.5 Gpa and 1260°C).

In view of the above problems, if foam-like porous diamond can be prepared, it will be beneficial for improving the holding force of the binder on diamonds. Compared with the coarse cutting-edge of ordinary diamonds, there are numerous small cutting edges on surface of the porous diamonds, which can disperse grinding stress and refine grinding lines. Under relatively lower pressure, porous diamonds can produce new cutting edges via local crushing, thus stabilizing and maintaining the high-efficiency and high-quality machining of the tool.

In this study, Fe/Fe_2O_3 was used to corrode diamonds at 950°C, and the porous diamonds were prepared after corrosion and acid pickling (our published research [20]). The conditions required for synthetic production of porous diamonds are relatively simple, and industrial production of the single particle porous diamonds is possible following our study. We have carried out an in-depth and detailed investigation on the diamond with porous structure. The morphology of the diamonds after corrosion was analyzed by SEM (scanning electron microscope). The particle size, pore volume and specific surface area of the diamonds before and after corrosion treatment were analyzed by laser particle size analyzer and BET (Brunauer-Emmett-Teller). The wettability of vitrified bonds to diamonds was analyzed by SEM (scanning electron microscope), wetting angle, XPS (X-ray photoelectron spectroscopy), zeta potential and EDS (Energy dispersive spectroscopy). The properties of vitrified bonds/diamonds composites were analyzed by porosity, density, bending strength and hardness. The grinding performance of the grinding tool was analyzed by comparing the surface roughness of silicon wafers before and after grinding. The grinding mechanism of the grinding tool was analyzed by comparing the SEM images of the grinding tool surface before and after grinding. Up till now, there has not been any research studies performed on the bonding properties of vitrified bonds with porous diamonds nor on the grinding performance of porous diamond abrasive tools. Our study provides new ideas for the application of the innovative high-performance porous diamond abrasive tools.

2. Materials And Methods

2.1. Materials

The ordinary diamonds (d_{50}: 45.26 μm) were purchased from Huanghe whirlwind company, China. Fe powders (grain size 1-2 μm) and Fe_2O_3 powders (grain size 1-2 μm) were obtained from Changsha Guoguang cemented carbide Co., Ltd., China. Concentrated nitric acid, concentrated hydrochloric acid, SiO_2, H_3BO_3, Al_2O_3, Li_2CO_3, Na_2CO_3, MgO, $ZrSiO_4$ and dextrin (all analytical purity) were from Sinopharm Chemical Reagent Co., Ltd. Diamond film (deposited on Si wafer by CVD, film size: 30mm x 30mm x 1mm) was obtained from Hebei Pressman Diamond Technology Co., Ltd., China. Silicon wafers were

obtained from Guangzhou Guifeng Electronic Technology Co., Ltd., China (surface roughness of 2.58 μm).

2.2. Experiments

2.2.1. Preparation of the porous diamonds

The synthetic diamond powders, Fe powders, and Fe_2O_3 powders were mixed with a ball mill at a mass ratio of 1:3:3 under the protection of argon at one atmospheric pressure. The uniformly mixed powders were pressed into a block at 30MPa, placed in a high temperature resistant corundum crucible, and then put into a tube furnace. Under the protection of argon at one atmospheric pressure, the sample was heated to 950°C (the heating rate: 5°C/min). After holding at 950°C for 4 h in the furnace, the tube furnace was switched off and the sample was allowed to cool in the furnace. During the cooling process, argon gas protection was maintained in the furnace.

After heat treatment, samples were acid washed with aqua regia for 1 h to remove the residual Fe and Fe_2O_3. Then, the powders were washed by deionized water until neutralized. The powders were dried and the porous diamonds were obtained.

The porous diamond film was prepared by uniformly spreading the corrosive agent on the diamond film. Thermochemical corrosion and pickling were carried out with the same process that was used to prepare the above-mentioned porous diamond particles.

2.2.2. Preparation of diamond abrasive tools

The basic binder was consisted of Al_2O_3-B_2O_3-MgO-ZrO_2-SiO_2-Na_2O-Li_2O. The corresponding chemicals are uniformly mixed at a certain proportion and put in high temperature resistant corundum crucible, heated in a muffle furnace to 1300 ℃ for 2 hours, and then quenched with water. The broken pieces of binder were ball milled, dried and passed through a 200-mesh sieve to obtain binder powders.

The diamonds, vitrified bonds, and dextrins were uniformly mixed according to the mass fraction ratio of 81:16:3. Then they were pressed into molds to form a 30mm×6mm×6mm sample strip and a φ 21mm×6mm cylinder (molding pressure 60MPa, pressure holding time 3min). Next, the samples were heated to 670°C (the heating rate: 3°C/min) and held for 1.5h to obtain the vitrified bond/diamond composite samples.

2.2.3. Monocrystalline silicon wafer grinding experiment

A VG401MK type ultra-precision grinding machine (Okamoto, Japan) was used to grind monocrystalline silicon. The grinding disc used in the grinding test was made of two kinds of diamonds (ordinary diamonds and porous diamonds). The grinding test piece was a ϕ 200mm × 725μm monocrystalline silicon wafer, the grinding disc speed was 1000r/min, the silicon wafer speed was 120r/min, and the feed rate was 50μm/min.

2.3. Characterization

SEM was used to observe the microscopic morphology of the diamond particles before and after corrosion, the bonding morphology between binder and diamond particle, the surface of the silicon wafer after grinding, and the surface of the abrasive tool after grinding (model: QUANTA-200, FEI Company of The Netherlands). The element distribution at the interface between binder and diamond was analyzed by energy dispersive spectroscopy (EDS) (model: Genesis 2000, EDAX, USA). A laser particle size analyzer was used to measure diamond grain size (model: SCF-106, OMEC Instruments Co., Ltd., China). The zeta potential of diamond surface is measured by Zeta potential analyzer (model: SurPASS Zeta, Antpedia, Austria). The Brunauer-Emmett-Teller (BET) instrument was used to analyse the pore volume and specific surface area of diamonds (model: 3H-2000PS1, Beijing BSD Instrument Technology Co., Ltd., China). The wetting angle of the binder on the diamond film was measured by a high temperature contact angle tester (model: Theta Flex HPC, Biolin, Finland). The XPS was used to characterize the chemical bonding state of C elements on the surface of the ordinary diamonds and porous diamonds (model: K-Alpha, Thermo Scientific, American). A Rockwell hardness tester was used to measure the hardness of the vitrified bond/diamond composites (model: HR-150DT, Shanghai Shangcai testing machine Co., Ltd., China). An electronic universal testing machine (model: WDW-1, Shanghai Songdun Instruments Manufacturing Co., Ltd., China) was used to detect the three-point bending strength of the sintered body of the vitrified bond/diamond composites. The density and porosity of the vitrified bond/diamond composites were analyzed by the Archimedes drainage method. A white light interferometer (model: NewView 7100, ZYGO, USA) was used to measure the surface roughness of the silicon wafer.

3. Results And Discussion

3.1. Micro morphology, particle size, pore volume and specific surface area of the ordinary diamonds and porous diamonds

The surfaces of the ordinary diamonds are angular, smooth and without obvious defects (Fig. 1a). There are numerous of micro and nano cutting edges and holes on the surfaces of the porous diamonds (Fig. 1b, c). In addition, the grain size of diamonds was reduced after corrosion treatment, and the pore volume and specific surface area were greatly increased (Table 1), which was conducive to increasing the contact area between the binder and the porous diamonds, thereby increasing the holding force of the binder to the diamonds. The porous skeleton structure can significantly improve the self-sharpening property of the abrasives.

Table.1. Diamond particle size, specific surface area, and pore volume.

Test items	Diamond size d_{50}	Diamond specific surface area	Diamond pore volume
The ordinary diamond	45.26 μm	0.187 m^2/g	0.000 ml/g
The porous diamond	38.69 μm	4.435 m^2/g	0.145 ml/g

3.2. Analysis of the bonding performance between the vitrified bonds and diamonds

3.2.1. The wettability of the vitrified bond to diamonds

A small amount of diamonds were scattered on the surface of the binder block, and then heated to sintering temperature to observe the wetting status between the binder and diamonds. The interface between the binder and the ordinary diamond was relatively straight and clear, and the ordinary diamond particle was exposed on vitrified bond matrix (Fig. 2a). The results showed that vitrified bond has poor wettability to the ordinary diamonds. Under the interfacial tension between the molten binder and the porous diamond abrasive, the binder climb onto the abrasive and the porous diamond was almost entirely submerged in the binder (Fig. 2b). The wettability of the binder to the porous diamond improved significantly.

3.2.2. Wetting angle of the vitrified bond to diamonds

Since it is difficult to accurately and directly measure the contact angle between the binder and the diamond, a relatively equivalent replacement was used to measure the contact angle between the binder and the diamond film at the sintering temperature [8]. The surface morphology of the porous diamond film is shown in Fig. 3. The results showed that the wetting angle of binder to the ordinary diamond film was 64°, and the wetting angle of the binder to the porous diamond film was 29 °, which was an approximately 35 ° reduction (Fig. 4).

3.2.3. EDS at the interface between the diamonds and the vitrified bond

The element distribution of the cross section of the vitrified bond/diamond composite was analyzed. The results showed that Zr, Al, Mg and Na elements were significantly enriched at the interface between the porous diamonds and the binder (Fig. 5a). However, the Zr, Al, Mg and Na elements were weakly enriched at the interface between the ordinary diamonds and the binder (Fig. 5b).

3.2.4. XPS analysis of C element on the diamond surface

In order to further analyze the reasons for the improvement in wettability between the binder and the porous diamonds, the C hybrid orbital states at the surface of the ordinary diamonds and porous

diamonds were studied by XPS.

Figure 6a shows the XPS spectra of the ordinary diamonds. The C 1s peak is located at 284.8 eV. The spectral line shape of the ordinary diamond indicates that it is composed of several components. The spectra were thus curve-fitted into two components with a Gaussian line shape. The binding energy of 284.7 eV was attributed to the sp^2 carbon bands and the binding energy of 285.2 eV was attributed to the sp^3 carbon bands [17, 21, 22].

Figure 6b shows the XPS spectra of the porous diamonds prepared in our experiment. The C 1s photoemission spectra revealed that significant structural changes occurred after corrosion, which was correlated with an significant increase of the sp^2 carbon bands in the C 1s XPS spectra. This was likely because the corrosive agent caused lattice distortion of C on the diamond surface to produce a layer of diamond-like carbon [23–26]. Diamond like carbon (DLC) is a metastable material formed by the combination of SP^3 and SP^2 bonds.

3.2.5. Zeta potential of diamond surface

There were a few SP^2 C atom bondings on the surface of the ordinary diamonds [27–29]. There were more SP^2 C atom bondings on the surface of the porous diamonds. The C atom of the SP^2 hybrid orbital formed C=C, and the C=C had one σ bond and one π bond. The π bond tended to bond with electrons from other atoms, making the diamond surface electronegative [30–32]. Therefore, the electronegativity of the porous diamond surface was stronger than that of the ordinary diamond surface (Fig. 7). The positively charged ions (Zr^{4+}, Al^{3+}, Mg^{2+} and Na^{+}) can diffuse to the negatively charged diamond surface due to their large number of positive charges, resulting in the enrichment of the positively charged ions on the diamond surface. The surface of the porous diamonds had higher electronegativity, thus the ability to attract the positively charged ions was enhanced and the wettability of the binder to the porous diamonds was improved.

Due to the large number of holes in the surface of the porous diamonds, the vitrified bond infiltrated into the porous diamonds under capillary action, which also enhanced the wettability of the binder to the porous diamonds. In summary, the wettability of the binder to the porous diamonds was improved through two ways (Fig. 8): 1. The capillary force generated by the pores [33]; 2. Enrichment of the positively charged ions on the surface of the porous diamonds .

3.3. Performance characterization of vitrified bond/diamond composites

3.3.1. Porosity, density, hardness and bending strength of composites

Compared with the vitrified bond/ordinary diamond composites, the hardness of the vitrified bond/porous diamond composites increased by about 22%, the bending strength decreased, the porosity increased, and the density decreased (Table 2). For the diamond abrasive tools, the hardness of the sintered complex is an important index that can measure the holding force of the binder on the diamonds. The hardness of the composite indicates that the diamond abrasives will not easily detach from the vitrified bond under the load of the indenter. The higher the hardness, the harder it is for the diamonds to detach from the vitrified bond matrix, and the higher the holding force of the binder on the abrasives. The porous diamonds have larger surface area and higher surface energy, which is beneficial for improving the wettability of the binder to the diamond abrasives. On the one hand, porous diamonds can enhance the mechanical holding force of the binder through their own foam holes. On the other hand, the chemical adsorption of the positively charged ions on the surface of porous diamond can enhance the chemical holding force of the binder. Therefore, the hardness of vitrified bond/porous diamond composite material can be increased.

Table.2. The vitrified bond/diamond composite porosity, density, Hardness, and bending strength.

Test items	Porosity	Density	Hardness	Bending strength
The vitrified bond/ordinary diamond composite	20%	2.23 g/cm^3	90 HRB	93 Mpa
The vitrified bond/porous diamond composite	28%	2.01 g/cm^3	110 HRB	85 Mpa

3.3.2. SEM of fracture of the vitrified bond/porous diamond composites

With the same proportion of binder and the same sintering temperature, the porosity of the vitrified bond/porous diamond composite was greater than that of the vitrified bond/ordinary diamond composite (Table 2). This was because during the sintering process of the vitrified bond/ordinary diamond composite, the molten binder only filled the pores between the diamond abrasives. However, in the sintering process of the vitrified bond/porous diamond composite, the melted binder at high temperature first filled the gaps between the porous diamond abrasives, and then some of the binder flowed into the pores of the porous diamond. As a result, the shrinkage of the samples was small during the sintering process. Compared with the vitrified bond/ordinary diamond composites, the pore size and distribution of the vitrified bond/porous diamond composites were relatively uniform (Fig. 9a, b). During the grinding process, the pores mainly played a role in increasing chip holding capacity and reducing the grinding temperature. Proper porosity can also effectively inhibit crack propagation and improve the grinding efficiency, impact strength and service life of abrasive tools [34]. For the composite test strips, the porosity had a greater influence on the bending strength of the material, and the bending strength of the

vitrified bond/porous diamond composite was lower than that of the vitrified bond/ordinary diamond composite.

3.4. Diamond abrasive tools grinding test

3.4.1. Surface morphology and roughness of silicon wafer after grinding

There were no large and deep scratches on the surface of the silicon wafer after grinding with the porous diamond abrasive tool. The consistency of the surface processing was improved (Fig. 10a, 11a), and the surface roughness Ra was 0.316μm. Large and deep scratches appeared on the surface of the silicon wafer after grinding with the ordinary diamond abrasive tool. The consistency of the surface processing was poor (Fig. 10b, 11b), and the surface roughness was 0.436μm.

Porous diamonds have a higher number of cutting edges than ordinary diamonds. In the grinding process, micro-edge cutting and micro-edge fragmentation will occur in porous diamonds, which helps to achieve self-sharpening in porous diamonds through local crushing. Porous diamond abrasive tools have more cutting edges per unit area. The more nicks per unit area that can be processed, the better the contour of the nicks and the smaller the surface roughness of the workpiece.

3.4.2. SEM of diamond grinding tool surface after grinding

There were many pits on the surface of the ordinary diamond grinding tools after grinding (Fig. 12a, b), which were caused by insufficient holding force of the binder to the ordinary diamonds. The detached diamonds easily scratched the surface of the machined workpiece. The surface of the porous diamond tools after grinding was smooth without pits (Fig. 12c, d), which indicates that the particles did not detach in their entirety during the grinding process due to the high holding force of the binder on the porous diamonds. The diamonds all failed in a broken off manner. The results show that the binder has a higher holding force on porous diamonds, and the porous diamond tool has better shape retention.

3.4.3. Grinding performance and grinding mechanism of diamond grinding tools

Compared with ordinary diamond abrasives, the grinding efficiency of porous diamond abrasives increased by 29.6% and the grinding ratio decreased by 15.5% (Table 3). There was a large difference between the cutting edges of the ordinary diamonds and porous diamonds. The ordinary diamond abrasive particles had large single cutting edges, whereas the porous diamond abrasives had micro-and nano-scale multi-cutting edges. For porous diamonds, the size of their cutting edges became smaller, the number of the cutting edges increased, the grinding heat and stress were dispersed, the cutting depth of the edges was reduced, the cutting damage was effectively reduced and the surface processing quality was improved. The embedding effect of the binder into the porous diamonds allowed the abrasive particles to stay attached in the surface of abrasive tool. When grinding pressure was applied, the outer cutting edges of the porous diamonds were worn away, then new cutting edges were exposed to continue

grinding. Porous diamond abrasive particles were broken locally layer by layer, rather than the disorderly breaking of ordinary diamond abrasive particles or detaching from the binder matrix (Fig. 13). Porous diamond abrasives have higher self-sharpness, and the utilization rate and grinding efficiency of porous diamond are better than ordinary diamonds. However, as the strength of porous diamond particles decreases, the durability and grinding ratio of porous diamond tools will also decrease.

Table.3. Grinding performance of diamond abrasive tools

Test items	Grinding efficiency	Grinding ratio	Silicon wafer surface Ra
The ordinary diamond abrasive tool	2.7 g/h	7.23	0.436 μm
The porous diamond abrasive tool	3.5 g/h	6.11	0.316 μm

4. Conclusions

A method for preparing single grain porous diamonds was developed by using Fe/Fe_2O_3 in thermochemical corrosion process. XPS indicated that some SP^2 hybrid C atoms were generated on the surface of the porous diamonds after corrosion. SEM, EDS, wettability angle and Zeta potential indicated that the porous framework and the enrichment of Zr^{4+}, Al^{3+}, Mg^{2+} and Na^{+} on the surface of the porous diamonds can significantly improve the wettability of the binder to the porous diamonds, and thus improve the holding force of the binder on the porous diamonds. Grinding experiments showed that the porous diamonds had a high self-sharpening property. Compared with ordinary diamond abrasive tools, porous diamond abrasive tools showed a 29.6% increase in grinding efficiency, a 15.5% decreased in grinding ratio, a 27.5% reduction in workpiece surface roughness. The micro-edge cutting and micro-edge breaking of porous diamonds significantly improved the grinding efficiency and precision, which greatly improved the surface quality of the machined workpiece.

Declarations

Conflict of Interest

The authors have declared that they have no conflicts of interest pertaining to this study.

Acknowledgments

The authors of this paper are grateful for the financial support from the National Natural Science Foundation of China (Grant No. 751229124), the State Key Laboratory of Advanced Technology for Materials Synthesis and Processing (Grant No. 2021-KF-6), the Key Research and Development Project of

Guangxi Guilin (Grant No. AB20159010) and the Scientific Research Project of Education Department of Hunan Province (Grant No. 19C0605).

References

1. Miao W, Ding Y, Zhao Y, et al. Modified gel casting technique to fabricate honeycomb structured vitrified-bonded ultrafine diamond grinding wheels. Ceram Int. 2020;46:4462–9. Doi:10.1016/j.ceramint.2019.10.172.
2. Souza AM, Silva EJ. Global strategy of grinding wheel performance evaluation applied to grinding of superalloys. Precis Eng. 2019;57:113–26. Doi:10.1016/j.precisioneng.2019.03.013.
3. Lin T, Liu S, Ji Z, et al. Vitrified bond diamond grinding wheel prepared by gel-casting with 3D printing molds. Diam Relat Mater. 2020;108:107917. Doi:10.1016/j.diamond.2020.107917.
4. Chuang TK, Tsai YT, Lin KH. Effects of added nano titanium on the microstructure and mechanical properties of vitrified bond diamond tools. International Journal of Refractory Metals Hard Materials. 2018;74:107–13. Doi:10.1016/j.ijrmhm.2018.03.013.
5. Radetzky M, Heß P, Fiur P, et al. The influence of contact force variation on surface topographies within high precision cutlery fine grinding. Procedia CIRP. 2021;101:186–9. Doi:10.1016/j.procir.2021.02.021.
6. Kakinuma Y, Konuma Y, Fukuta M, et al. Ultra-precision grinding of optical glass lenses with La-doped CeO_2 slurry. CIRP Ann. 2019;68:345–8. Doi:10.1016/j.cirp.2019.04.089.
7. Wu B, Zhao B, Ding W, et al. Investigation of the wear characteristics of microcrystal alumina abrasive wheels during the ultrasonic vibration-assisted grinding of PTMCs. Wear. 2021;477:203844. Doi:10.1016/j.wear.2021.203844.
8. Chen SP, Liu XP, Wan L, et al. Effect of V_2O_5 addition on the wettability of vitrified bond to diamond abrasive and grinding performance of diamond wheels. Diam Relat Mater. 2020;102:107672. Doi:10.1016/j.diamond.2019.107672.
9. Zhao B, Zhao CY, Gao G. Research on the Topography Features of the Densely Bonded Diamond Grinding Wheel Dressed by Elliptical Ultrasonic Vibration. Adv Mater Res. 2011;188:330–5. Doi. 10.4028/www.scientific.net/AMR.188.330.
10. Flegner P, Kačur J, Durdán M, et al. Significant damages of core diamond bits in the process of rocks drilling. Eng Fail Anal. 2016;59:354–65. Doi:10.1016/j.engfailanal.2015.10.016.
11. Wu S, Zhang F, Ni Y, et al. Grinding of alumina ceramic with microtextured brazed diamond end grinding wheels. Ceram Int. 2020;46:19767–84. Doi:10.1016/j.ceramint.2020.05.009.
12. Grabchenko AI, Romashov DV. Simulation of the effect of sintering on the integrity of diamond grains in grinding wheels. Nanotechnology Perceptions. 2014;10:42–53. Doi:10.4024/N06GR14A.ntp.010.01.
13. Choudhary A, Paul S. Surface generation in high-speed grinding of brittle and tough ceramics. Ceram Int. 2021;47:30546–62. Doi. 10.1016/j.ceramint.2021.07.233.

14. Dhandapani VS, Kang KM, Seo KJ, et al. Enhancement of tribological properties of DLC by incorporation of amorphous titanium using magnetron sputtering process. Ceram Int. 2019;45:11971–81. Doi. 10.1016/j.ceramint.2019.03.090.
15. Chu K, Liu Z, Jia C, et al. Thermal conductivity of SPS consolidated Cu/diamond composites with Cr-coated diamond particles. J Alloy Compd. 2010;490:453–8. Doi:10.1016/j.jallcom.2009.10.040.
16. Liu XP, Song DD, Wan L, et al. Influence of heat treatment temperature on bonding and oxidation resistance of diamond particles coated with TiO_2 film. Bull Mater Sci. 2015;38:1263–70. Doi:10.1007/s12034-015-1009-6.
17. Liu K, Lv Z, Dai B, et al. High-selectivity anisotropic etching of single-crystal diamond by H plasma using iron catalysis. Diam Relat Mater. 2018;86:186–92. Doi:10.1016/j.diamond.2018.04.026.
18. Sheng LX, Chen CK, Jiang MY, et al. The effects of microwave oxygen plasma treatments on the microstructure and Ge-V photoluminescent properties of diamond particles. Chinese Physics B 2020, 29. Doi:10.1088/1674-1056/ab8db0.
19. Wang J, Su Y, Tian Y, et al. Porous single-crystal diamond. Carbon. 2021;183:259–66. Doi:10.1016/j.carbon.2021.06.083.
20. Li JW, Liu XP, Wan L, et al. Using the thermochemical corrosion method to prepare porous diamonds. Ceramics International; 2021. Doi:10.1016/j.ceramint.2021.09.041.
21. Pu JC, Wang SF, Sung JC. High-temperature oxidation behavior of nanocrystalline diamond films. J Alloy Compd. 2010;489:638–44. Doi:10.1016/j.jallcom.2009.09.140.
22. Zhu C, Cui C, Wu X, et al. Study on surface modification of diamond particles and thermal conductivity properties of their reinforced metal-based (Cu or Mg) composites. Diam Relat Mater. 2020;108:107998. Doi:10.1016/j.diamond.2020.107998.
23. Liu Y, Erdemir A, Meletis EI. A study of the wear mechanism of diamond-like carbon films. Surface Coatings Technology. 1996;82:48–56. Doi:10.1016/0257-8972(95)02623-1.
24. Allen M, Myer B, Rushton N. In vitro and in vivo investigations into the biocompatibility of diamond-like carbon (DLC) coatings for orthopedic applications. Journal of Biomedical Materials Research 2001, 58: 319–328. Doi:10.1002/1097-4636(2001)58:3<319::AID-JBM1024>3.0.CO;2-F.
25. Qi J, Chen D, Wang Y, et al. Effects of pulse width on corrosion behavior of diamond-like carbon coatings prepared on the surface of high nitrogen nickel-free stainless steel. Surf Rev Lett 2021, 28. Doi:10.1142/S0218625X21500323.
26. Elam FM, Hsia FC, Van S, et al. The influence of corrosion on diamond-like carbon topography and friction at the nanoscale. Carbon. 2021;179:590–9. Doi:10.1016/j.carbon.2021.04.068.
27. Kozak H, Remes Z, Houdkova J, et al. Chemical modifications and stability of diamond nanoparticles resolved by infrared spectroscopy and Kelvin force microscopy. J Nanopart Res. 2013;15:1568. Doi:10.1007/s11051-013-1568-7.
28. Jirásek V, Čech J, Kozak H, et al. Plasma treatment of detonation and HPHT nanodiamonds in diffuse coplanar surface barrier discharge in H_2/N_2 flow. physica status solidi (a). 2016;213:2680–

6. Doi:10.1002/pssa.201600184.
29. Zhuk TS, Koso T, Pashenko AE, et al. Toward an Understanding of Diamond sp^2-Defects with Unsaturated Diamondoid Oligomer Models. J Am Chem Soc. 2015;137:6577–86. Doi:10.1021/jacs.5b01555.
30. Mo Y, Zhang Y, Gao J. A Simple Electrostatic Model for Trisilylamine: Theoretical Examinations of the n→σ* Negative Hyperconjugation, pπ→dπ Bonding, and Stereoelectronic Interaction. Journal of the American Chemical Society 1999, 121. Doi:10.1021/ja9904742.
31. Wang H, Wang W, Jin WJ. σ-Hole Bond vs π-Hole Bond: A Comparison Based on Halogen Bond. Chem Rev. 2016;116:5072–104. Doi:10.1021/acs.chemrev.5b00527.
32. Flister M, Timerghazin QK. Structure, Stability, and Substituent Effects in Aromatic S-Nitrosothiols: The Crucial Effect of a Cascading Negative Hyperconjugation/Conjugation Interaction. The Journal of Physical Chemistry A. 2014;118:9914–24. Doi:10.1021/jp5079136.
33. Choi H, Liang H. Wettability and spontaneous penetration of a water drop into hydrophobic pores. J Colloid Interface Sci. 2016;477:176–80. Doi:10.1016/j.jcis.2016.05.029.
34. Dong S, Wang Y, Ashour A, et al. Nano/micro-structures and mechanical properties of ultra-high performance concrete incorporating graphene with different lateral sizes. Compos Part A: Appl Sci Manufac. 2020;137:106011. Doi:10.1016/j.compositesa.2020.106011.

Figures

Figure 1

SEM of diamonds before and after corrosion: (a) ordinary diamond, (b) porous diamonds, (c) partial enlarged view of (b).

Figure 2

The bonding morphology between the vitrified bond and the diamond particle: (a) ordinary diamond, (b) porous diamond.

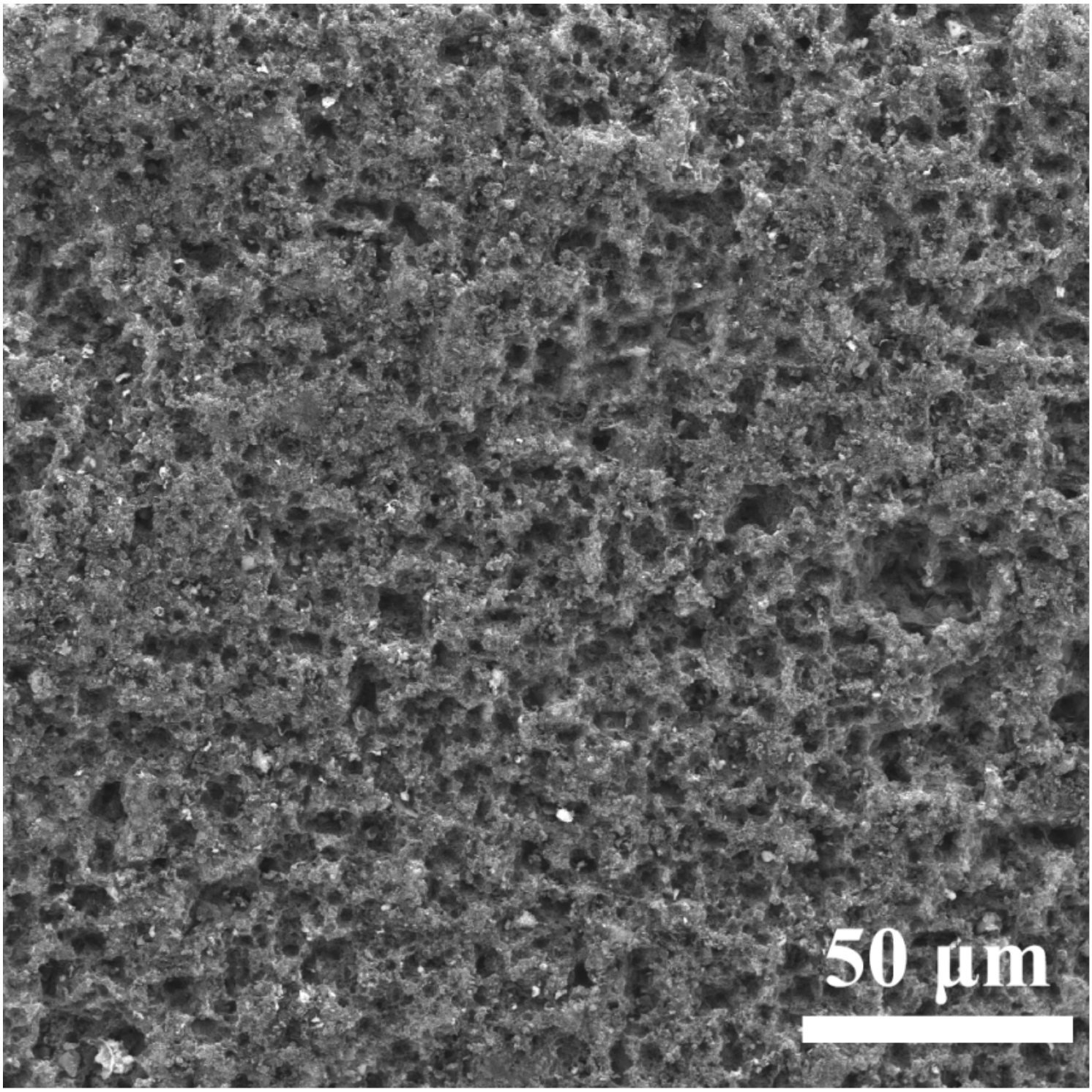

Figure 3

SEM of porous diamond film.

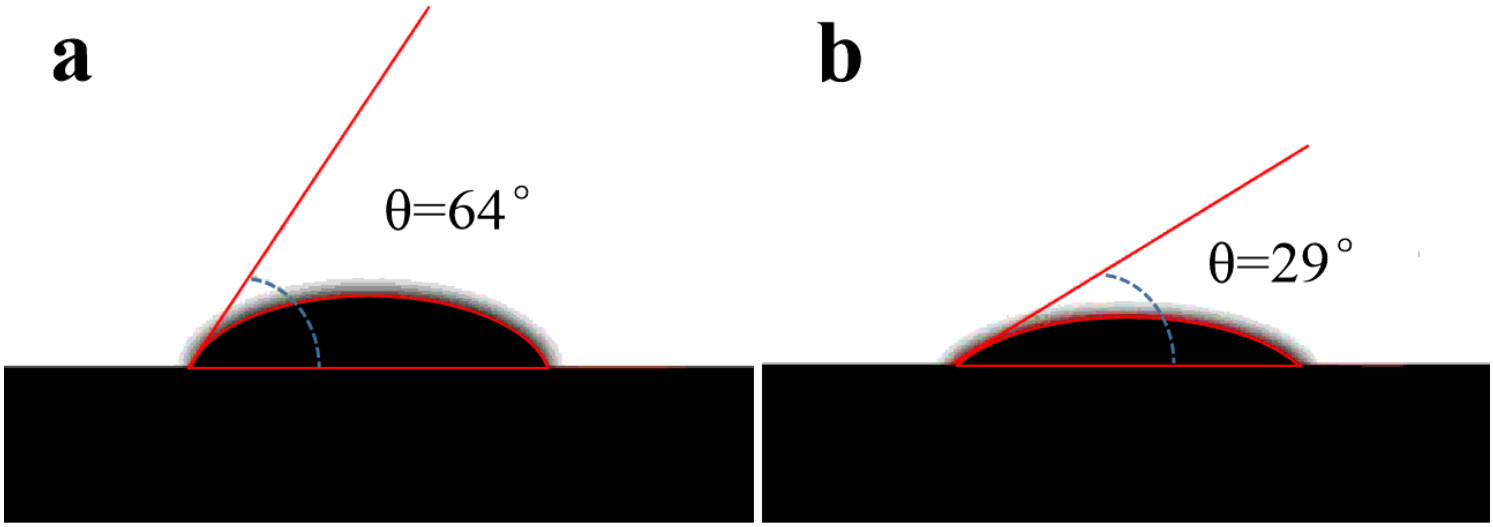

Figure 4

The wetting angle of the vitrified bond on the diamond film: (a) ordinary diamond, (b) porous diamond.

Figure 5

The element distribution at the interface between the vitrified bond and the diamond: (a) porous diamond, (b) ordinary diamond.

Figure 6

XPS of C elements on the diamond: (a) ordinary diamond, (b) porous diamond.

Figure 7

Zeta potential on diamond surface.

Figure 8

Mechanism of interfacial wettability.

Figure 9

Fracture surface micrograph of vitrified bond/diamond: (a) porous diamond, (b) ordinary diamond.

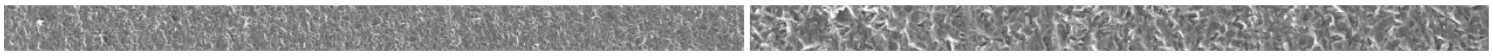

Figure 10

Micrograph of silicon wafer after grinding: (a) silicon wafer ground by porous diamond abrasive tool, (b) silicon wafer ground by ordinary diamond abrasive tool.

Figure 11

Three-dimensional contour of (a) silicon wafer ground by porous diamond abrasive tool, (b) silicon wafer ground by ordinary diamond abrasive tool.

Figure 12

The surface morphology of the diamond abrasive tools after grinding: (a) ordinary diamond abrasive tool (low magnification), (b) ordinary diamond abrasive tool (high magnification), (c) porous diamond abrasive tool (low magnification), (c) porous diamond abrasive tool (high magnification).

Figure 13

The grinding mechanism of the diamond abrasive tools.